Intercomparison of wind-driven rain models based on a case study with full-scale measurements

The Fifth International Symposium on Computational Wind Engineering (CWE2010)
Chapel Hill, North Carolina, USA May 23-27, 2010

Intercomparison of wind-driven rain models based on a case study with full-scale measurements

B. Blocken [a], P.M. Briggen [a], H.L. Schellen [a], J. Carmeliet [b,c]

[a] *Building Physics and Systems, Eindhoven University of Technology, the Netherlands, b.j.e.blocken@tue.nl*
[b] *Chair of Building Physics, Swiss Federal Institute of Technology ETHZ, Zürich, Switzerland*
[c] *Laboratory for Building Technologies, Swiss Federal Laboratories for Materials Testing and Research, Empa, Dübendorf, Switzerland*

ABSTRACT: Three different calculation models for wind-driven rain (WDR) are compared: the semi-empirical model in the ISO standard for WDR (ISO), the semi-empirical model by Straube and Burnett (SB) and the CFD model by Choi, extended by Blocken and Carmeliet. This paper builds further on the comparison of these models for idealized building configurations and fixed wind and rain conditions in [*Blocken et al., 2010. Comparison of calculation models for wind-driven rain deposition on building facades, Atmospheric Environment 44(14): 1714-1725*]. In the present paper, these models are applied to a high-rise monumental tower building, for a transient rain event, and the model results are compared with full-scale measurements. The agreement between the CFD results and the measurements is quite good at the upper part of the facade, while the ISO and SB model show large discrepancies at these facade positions.

1 INTRODUCTION

Three different calculation models for wind-driven rain (WDR) on buildings are compared: the semi-empirical model in the ISO Standard for WDR (ISO, 2009), the semi-empirical model by Straube (1998) and Straube and Burnett (2000) and the CFD model by Choi (1991, 1993, 1994) that was extended into the time domain by Blocken and Carmeliet (2002, 2007). These models are referred to as ISO, SB and CFD, respectively. The theory of the models and a comparison of model performance by application to generic, idealized buildings were provided in earlier studies (Blocken and Carmeliet 2010; Blocken et al. 2010). In the present paper, the models are applied to determine the spatial and temporal distribution of WDR on the south-west facade of a real building for a real, transient rain event. This real building is the tower of the Hunting Lodge St. Hubertus, a monumental building in the national park "De Hoge Veluwe" in the Netherlands.

2 DESCRIPTION OF BUILDING, SURROUNDINGS AND MEASUREMENT SET-UP

The Hunting Lodge St. Hubertus consists of a low-rise rectangular volume with wings that stretch out diagonally and with a characteristic tower in the middle of the building (Fig. 1; Briggen et al. 2009). The total building height is 34.5 m. From the fourth floor up, the tower is rectangular with dimensions 4.8 x 4.2 m^2. There are no other buildings in the immediate vicinity, but the building is surrounded by a forest. There is an elongated clear-cut in the forest, SW of the building, with a length of about 600 m. The aerodynamic roughness length z_0 of the forest is estimated 1 m, while that of the clear-cut is estimated 0.05 m. The measurement set-up consisted of

a meteorological mast positioned in such a way that it measured SW wind without disturbance by the building and the trees in its immediate vicinity (Briggen et al., 2009). The meteorological mast was equipped with an ultrasonic anemometer, providing the reference wind speed and wind direction at 10 m height: U_{10} and φ_{10}. Reference rainfall intensity R_h was measured by a rain gauge shielded by a wind screen. It was placed at the same location as the meteorological mast. WDR gauges (0.2 x 0.2 m² catch area, made of sheet glass according to the WDR gauge design guidelines by Blocken and Carmeliet (2006a)) were installed at the tower facades (Fig. 1). Most gauges were positioned on the SW facade, because SW is the prevailing wind direction. All data were gathered on a 1-minute basis and afterwards averaged over 10-minute intervals. More information can be found in (Briggen et al., 2009).

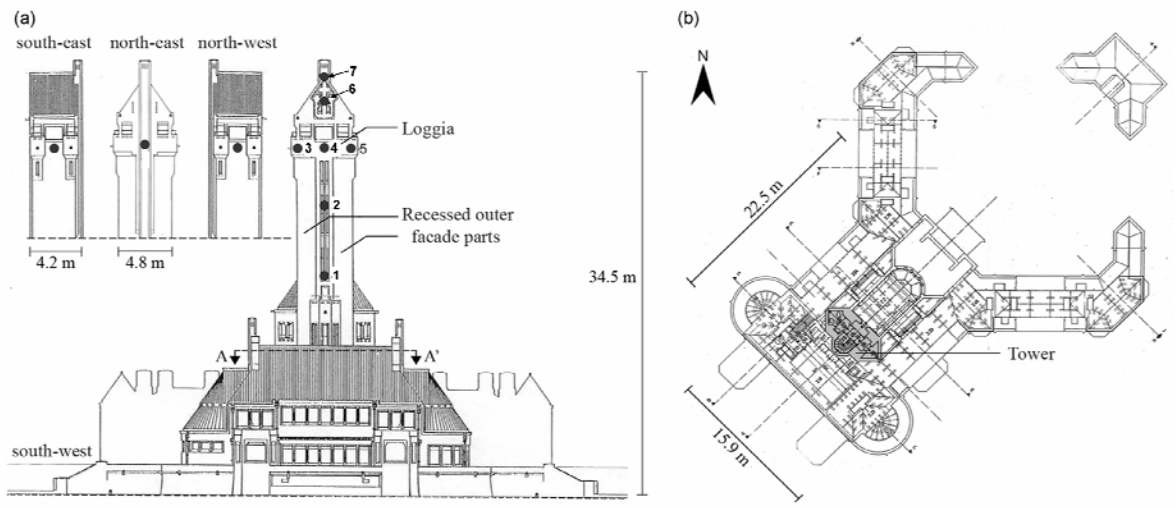

Figure 1. (a) South-west facade of Hunting Lodge St. Hubertus and the positions and numbers of the wind-driven rain gauges (1-5), and of two additional positions without gauges (6-7) at the SW facade; (b) cross section A-A' (indicated in Fig. 1a) of the building. Dimensions in meter.

3 WIND-DRIVEN RAIN MODELS

3.1 *Model equations*

The input meteorological data consist of 10-minute values of U_{10}, φ_{10} and R_h. These hourly or 10-minute intervals are called time steps. For the purpose of comparison, each model calculates the WDR intensity R_{wdr} for each time step by:

$$R_{wdr} = \alpha \cdot U_{10} \cdot R_h^{0.88} \cdot \cos\theta \quad (1)$$

where α is the WDR coefficient and θ is the angle – in a horizontal plane – between the wind direction and the normal to the facade. Depending on the model, different expressions for α have to be used (Blocken and Carmeliet, 2010).

For wind perpendicular to the facade ($\theta = 0°$), the WDR coefficient in the CFD model is:

$$\alpha = \frac{\eta \cdot R_h^{0.12}}{U_{10}} \quad (2)$$

where η is the catch ratio from the CFD simulation, which is defined as the ratio R_{wdr}/R_h.

The WDR coefficient in the ISO model is:

$$\alpha = \frac{2}{9} \cdot C_R \cdot C_T \cdot O \cdot W \quad (3)$$

where C_R is the roughness coefficient, C_T the topography coefficient, O the obstruction factor and W the wall factor. C_R takes into account the change of mean wind speed at the site due to the height above the ground and the upstream roughness of the terrain. It is given by:

$$C_R(z) = K_R \ln\left(\frac{z}{z_0}\right) \quad \text{for } z \geq z_{min} \quad ; \quad C_R(z) = C_R(z_{min}) \quad \text{for } z < z_{min} \quad (4)$$

where z is the height above ground, K_R the terrain factor and z_{min} a minimum height. Values for these parameters are provided in the Standard (ISO, 2009). For example, for $z_0 = 0.01$ m: $K_R = 0.17$ and $z_{min} = 2$ m, and for $z_0 = 0.05$ m: $K_R = 0.19$ and $z_{min} = 4$ m. The topography coefficient takes into account the increase of mean wind speed over isolated hills and escarpments. The obstruction factor O takes into account the shelter of the wall by the nearest obstacle. The wall factor W tries to take into account the type of the wall (height, roof overhang) and the variation of WDR across the surface of the wall. Some values for W are shown in Figure 2a-c.

The WDR coefficient in the SB model is:

$$\alpha = DRF \,.\, RAF \,.\, \left(\frac{z}{10}\right)^{\beta} \cdot R_h^{0.12} \quad (5)$$

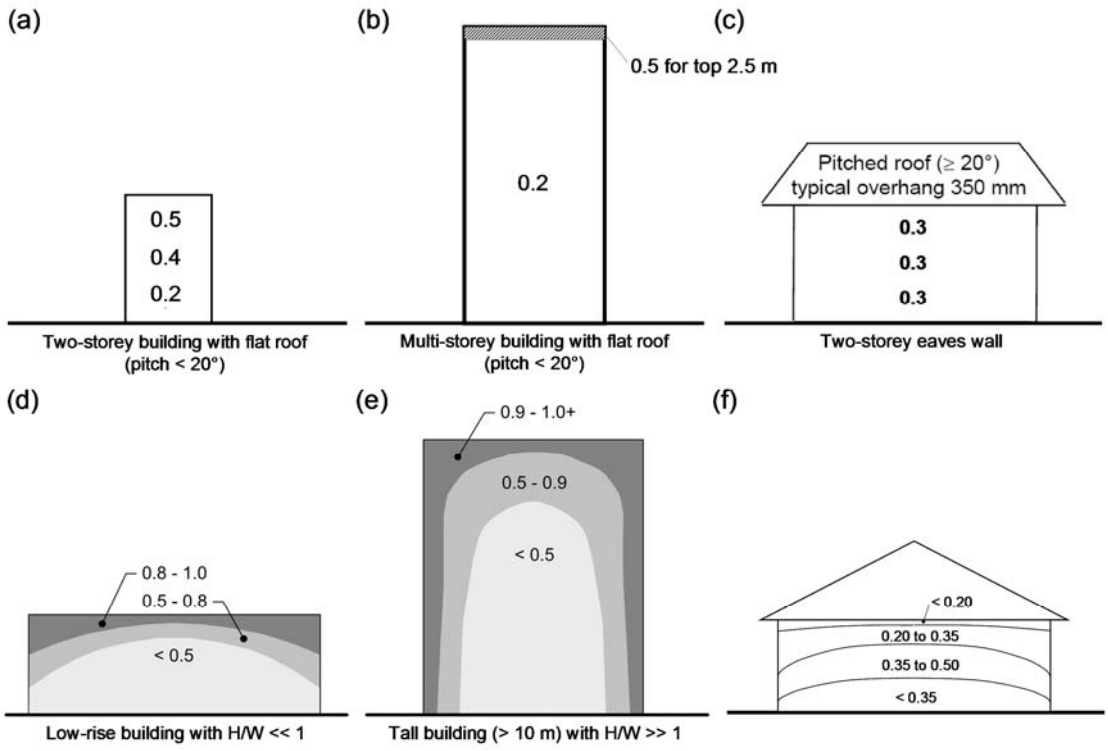

Figure 2. (a-c) ISO wall factors (W) on the windward facade of a two-storey building with flat roof, a multi-storey building with flat roof and a two-storey eaves building (modified from ISO (2009)); (d-f) Contours of Straube and Burnett's rain admittance factor (RAF) on the windward facades of a wide low-rise building with flat roof, a high-rise building and a low-rise building with pitched roof (Straube, 1998, Straube and Burnett, 2000).

where DRF is the driving rain function, RAF the rain admittance factor and β the power-law exponent corresponding to the terrain roughness of the building site. The RAF is constant in time, while the DRF varies in time. RAF values have been published by Straube (1998) and Straube and Burnett (2000), but only for three types of buildings: see Figure 2d-f. The DRF is calculated as the inverse of the terminal velocity of fall V_t, given by the equation by Dingle and Lee (1972):

$$V_t(d) = -0.166033 + 4.91844\,d - 0.888016\,d^2 + 0.054888\,d^3 \leq 9.20 \text{ m/s} \quad (6)$$

where d is the raindrop diameter. Concerning the choice of d, Straube and Burnett (2000) suggest the median diameter from the raindrop spectrum by Best (1950):

$$\bar{d} = 1.105\,R_h^{0.232} \quad (7)$$

For each model, the WDR sum (S_{wdr} in mm) for each time step is obtained by multiplying R_{wdr} with the time step length Δt. The accumulated (total) WDR at the end of the rain event is:

$$S_{wdr,tot} = \sum (R_{wdr} \cdot \Delta t) \quad (8)$$

3.2 *Main conclusions on model performance from previous studies*

The main conclusions from the previous comparison studies (Blocken and Carmeliet, 2010; Blocken et al., 2010) are summarized, below to support the analysis of model performance in this paper. The conclusions concern the ISO and SB model, when contrasted with the CFD model, which was shown to provide accurate results in validation studies (e.g. Blocken and Carmeliet, 2002, 2006b, Tang and Davidson, 2004, Abuku et al., 2009).

1 The ISO and SB model only provide information (factors W and RAF) for a few building types;
2 The ISO model does not take into account the variation of α along the width of the facade;
3 Instead of providing a single value for the RAF, the SB model provides a minimum and maximum limit. For some facade positions, these values bound a wide range, which limits the predictive capability of this model;
4 In the SB model, the RAF values at the top edge and vertical edge of the facade are too large, and for low R_h, the dependency of the DRF on R_h is too strong;
5 The wind-blocking effect (Blocken and Carmeliet, 2006b) is not reproduced by the ISO and the SB model. The wind-blocking effect refers to the decrease of upstream streamwise wind speed, and therefore also of the WDR intensity, with an increase of the building scaling length (BSL):

$$BSL = \left(B_L\,B_S^{\,2}\right)^{\frac{1}{3}} \quad (9)$$

where B_L is the larger and B_S is the smaller dimension of the windward facade. The BSL was defined by Wilson (1989) for estimating the dimensions of flow recirculation regions on building roofs.

6. The increase of α with increasing R_h can be reproduced by the CFD model. The ISO model does not predict this dependency, while the SB shows the opposite trend (decrease with increasing R_h).

4 MODEL APPLICATION

4.1 *CFD model*

3D steady RANS simulations with the realizable k-ε model (Shih et al., 1995) were performed with the commercial CFD code Fluent 6.3 by Briggen et al. (2009). The simulations were conducted following the CFD best practice guidelines by Franke et al. (2007) and Tominaga et al. (2008) and the recommendations by Blocken et al. (2007) for CFD simulation of neutral atmospheric boundary layer flow with this code. The simulation details, including the grid-sensitivity analysis, can be found in (Briggen et al., 2009). Simulations were only made for SW wind direction and for the SW facade ($\theta = 0°$). The raindrop trajectories, specific catch ratio and catch ratio were all calculated with author-written program codes (Blocken and Carmeliet, 2006b). The raindrop-size distribution by Best (1950) was adopted. The simulations were made for U_{10} = 1, 2, 3, 5 and 10 m/s and for R_h = 0.1, 0.5, 1, 2, 3, 4, 5, 6, 8, 10, 12, 15, 20, 25 and 30 mm/h. η and α (Eq. 2) were calculated at every position at the west facade (resolution 0.08 x 0.08 m²) for all the different combinations of U_{10} and R_h. These values for α are used in Eq. (1), together with the meteorological data of the rain event, to determine the WDR intensity at different facade positions. The WDR intensities are converted to the accumulated WDR $S_{wdr,tot}$ by Eq. (8).

4.2 *ISO model*

C_R, C_T and O are determined. CR is calculate using the parameters for terrain category II (ISO, 2009). C_T and O are equal to one in this case. The wall factors are taken from Figure 2b for a multi-storey building, although the ISO standard does not provide wall factors for a facade that is triangular at the top (Figure 1a).

4.3 *Model by Straube and Burnett*

The RAF values are taken from Figure 2e, which seems appropriate, because H >> W applies for the tower. However, these values are strictly not applicable for positions 6 and 7, situated at the triangular part of the facade. The value of β that corresponds to terrain category II in the ISO model is 0.16.

4.4 *Comparison of temporal distribution of wind-driven rain*

The rain event is shown in Figure 3a. It is characterized by a series of individual showers. Wind speed is on average 1.3 m/s and wind direction during rain is only slightly oblique to the SW facade ($\theta \approx 0°$). R_h ranges from 0 to 4.5 mm/h, and is on average equal to 1.2 mm/h (zero R_h values excluded). Figure 3b shows the measured and calculated temporal distribution of WDR at position 3. A conservative measurement error estimate is E_{wdr} = 0.2 mm (Briggen et al., 2009). All models qualitatively reproduce the temporal variation. Quantitatively, CFD somewhat underestimates the measured values. ISO provides an estimate that is about four times too low, while SBmin is larger than both the measurements and the CFD results. Figure 3c shows the temporal variation of α at the same position, and Figure 3d shows the variation with U_{10} and R_h at position 3. Note that the overall differences between α_{CFD} on one hand, and α_{ISO} and α_{SBmax} and α_{SBmin} on the other hand, are very large. The reason for this is discussed in the next section.

4.5 *Comparison of spatial distribution of wind-driven rain*

Figure 4 compares measurements and calculations at the end of the rain event, at the positions of the WDR gauges (1-5) and at two additional positions near the top of the facade (6-7).

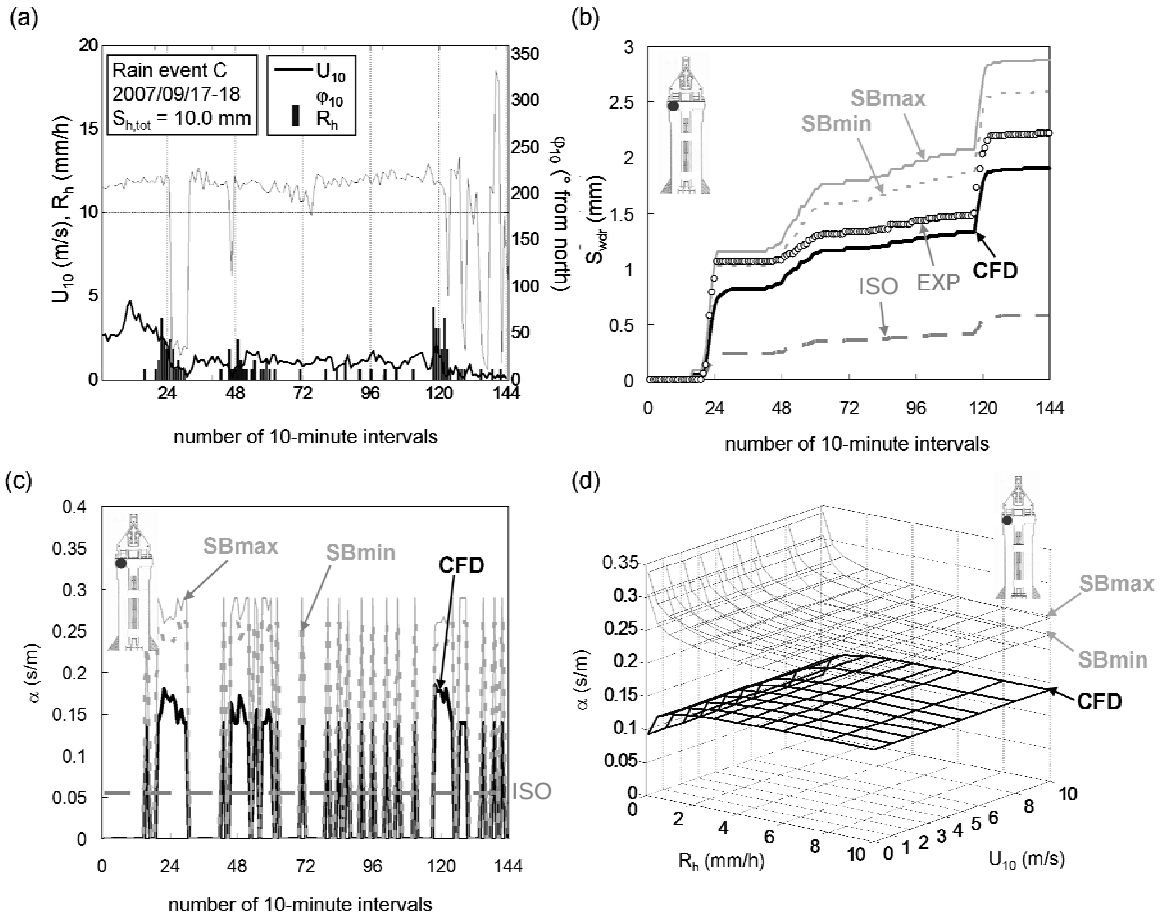

Figure 3. (a) Meteorological data record (10-minute data); (b) Temporal distribution of cumulative wind-driven rain at position 3 from experiments and CFD, ISO and SB models; (c) Temporal distribution of wind-driven rain coefficient α at position 3 for CFD, ISO and SB models; (d) Variation of α at position 3 with U_{10} and R_h according to CFD and SB model.

A conservative estimate for the error in the measured ratios is e_{wdr} = 0.02. The observations are:

1 Figure 4a: the measured ratios increase from bottom to top, and from the middle of the facade to the sides. The value at position 5 is slightly higher than at position 3, because the wind direction is a bit lower than 225° (= south-west). Data at position 2 are not available due to equipment malfunctioning.
2 Figure 4b: the CFD results also show the increase with height and from the middle to the sides. The agreement between CFD simulations and measurements is good, except at position 1. As mentioned by Briggen et al. (2009), this can be attributed to turbulent dispersion, which can have a significant effect in regions where the raindrop trajectories are almost parallel to the facade, which is the case at the lower part of high-rise buildings, such as near position 1.
3 Figure 4c: the results by the ISO model are up to four times smaller than the measurements. The same observation was made in Figure 3b. This poor performance appears to be in contradiction to the quite good performance by the ISO model for two idealized high-rise buildings in an earlier study (Blocken et al., 2010). The reason for this different performance is the wind-blocking effect (see statement nr. 5 in section 3.2). This effect is present in reality but not reproduced by the ISO model (Blocken et al., 2010). The larger the wind-blocking effect, the lower the WDR exposure of the facade. In the previous study, the BSL values were 50 m

and 31.7 m, while in the present study (when neglecting the wider bottom part of the building), the BSL is only 9.3 m. As a result, the actual WDR coefficients at this tower are much higher. Comparing CFD WDR coefficients has indeed shown that those for the present tower are about two to three times larger than those for the buildings in the previous study. The ISO model does not take the wind-blocking effect into account. Therefore, while it provides fairly good results for the high-rise buildings with BSL equal to 31.7 m and 50 m, it provides large underestimations for BSL = 9.3 m.

4 Figure 4d-e: SBmin and SBmax show the increase of WDR exposure with height and from the middle of the facade to the sides. Just like the ISO model, also the SB model does not take the wind-blocking effect into account. This could cause this model to also underestimate the WDR exposure. However, the SB model in general provides RAF values that are (much) too large in the vicinity of the top and side edges of high-rise buildings with rectangular facades (see statement 4 in section 3.2). These two effects compensate each other to some extent, but in spite of this, SBmin still overestimates the measurements at positions 3, 4 and 5. It also overestimates the CFD results at these positions. On the other hand, it does not overestimate the CFD values at positions 6 and 7. The reason is that these positions are in reality much more exposed, as the top of the facade is triangular (less wind-blocking) instead of rectangular. This causes a very high WDR exposure, as shown by the CFD results. The CFD value at the top is even larger than the value by SBmax. Note however, that strictly, the SB model does not provide wall factors for such positions at the top of triangular facades.

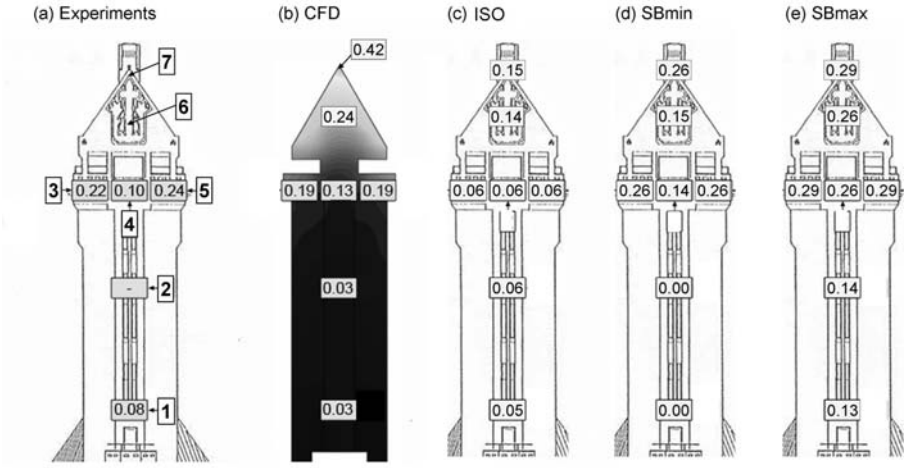

Fig. 4. Experimental and calculation results at end of the rain event in Figure 3a: spatial distribution of ratio of accumulated wind-driven rain to accumulated horizontal rainfall.

5 CONCLUSIONS

Three calculation models for wind-driven rain (WDR) have been compared by application to a real building and for a transient rain event: the ISO Standard for WDR (ISO), the Straube and Burnett model (SB) and the CFD model by Choi, extended by Blocken and Carmeliet (CFD). The main conclusions of the comparison are:

1 The agreement between measurements and CFD is quite good at the upper part of the building, while the discrepancies between the measurements and the ISO and SB models are large.

2 These discrepancies can be explained based on the six main conclusions from two previous studies. The main reasons however are the wind-blocking effect, which is reproduced by CFD but not by the ISO and SB models, and the fact that the SB model strongly overestimates the RAF at vertical and top edges of buildings.
3 The capabilities and deficiencies of the ISO and SB model, as identified in this paper, should be considered when applying these models for WDR deposition calculations.

6 REFERENCES

Abuku M., Blocken B., Nore K., Thue J.V., Carmeliet J., Roels S., 2009. On the validity of numerical wind-driven rain simulation on a rectangular low-rise building under various oblique winds. Building and Environment 44, 621– 632.

Best, A.C., 1950. The size distribution of raindrops, Quarterly Journal of the Royal Meteorological Society 76, 16-36.

Blocken, B., Carmeliet, J. 2002. Spatial and temporal distribution of driving rain on a low-rise building, Wind and Structures 5(5), 441-462.

Blocken, B., Carmeliet, J. 2006a. On the accuracy of wind-driven rain measurements on buildings, Building and Environment 41(12), 1798-1810.

Blocken, B., Carmeliet, J. 2006b. The influence of the wind-blocking effect by a building on its wind-driven rain exposure, Journal of Wind Engineering and Industrial Aerodynamics 94(2), 101-127.

Blocken, B., Carmeliet, J. 2007. On the errors associated with the use of hourly data in wind-driven rain calculations on building facades. Atmospheric Environment 41(11), 2335-2343.

Blocken, B., Stathopoulos, T., Carmeliet, J. 2007. CFD simulation of the atmospheric boundary layer: wall function problems, Atmospheric Environment 41(2), 238-252.

Blocken B., Carmeliet J., 2008. Guidelines for the required time resolution of meteorological input data for wind-driven rain calculations on buildings. Journal of Wind Engineering and Industrial Aerodynamics 96(5), 621-639.

Blocken B., Carmeliet J., 2010. Overview of three state-of-the-art wind-driven rain assessment models and comparison based on model theory. Building and Environment 45(3), 691-703.

Blocken, B., Deszö, G., van Beeck, J., Carmeliet, J. 2010. Comparison of calculation methods for wind-driven rain deposition on building facades. Atmospheric Environment 44(14), 1714-1725.

Briggen, P.M., Blocken, B., Schellen, H.L. 2009. Wind-driven rain on the facade of a monumental tower: numerical simulation, full-scale validation and sensitivity analysis, Building and Environment 44(8), 1675–1690.

Choi E.C.C., 1991. Numerical simulation of wind-driven-rain falling onto a 2-D building. Proceedings of Asia Pacific Conference on Computational Mechanics, Hong Kong, 1721-1728.

Choi, E.C.C., 1993. Simulation of wind-driven rain around a building. Journal of Wind Engineering and Industrial Aerodynamics 46&47, 721-729.

Choi, E.C.C. 1994. Determination of wind-driven rain intensity on building faces. Journal of Wind Engineering and Industrial Aerodynamics 51, 55-69.

Dingle AN, Lee Y. Terminal fall speeds of raindrops. Journal of Applied Meteorology 1972; 11: 877-879.

Franke, J., Hellsten, A., Schlünzen, H., Carissimo, B. 2007. Best practice guideline for the CFD simulation of flows in the urban environment. COST 732: Quality Assurance and Improvement of Microscale Meteorol. Models.

ISO, 2009. Hygrothermal performance of buildings – Calculation and presentation of climatic data – Part 3: Calculation of a driving rain index for vertical surfaces from hourly wind and rain data. ISO 15927-3:2009.

Shih, T.H., Liou, W.W., Shabbir, A., Zhu, J. 1995. A new k-ε eddy-viscosity model for high Reynolds number turbulent flows – model development and validation, Computers & Fluids 24(3), 227-238.

Straube, J.F. 1998. Moisture control and enclosure wall systems, Ph.D. thesis, Civil Engineering, University of Waterloo, Ontario, Canada, 318 p.

Straube, J.F., Burnett, E.F.P. 2000. Simplified prediction of driving rain on buildings, Proc. of the International Building Physics Conf., Eindhoven, The Netherlands, 18-21 September 2000, 375-382.

Tang W., Davidson C.I., 2004. Erosion of limestone building surfaces caused by wind-driven rain. 2. Numerical modelling. Atmospheric Environment 38(33), 5601-5609.

Tominaga, Y., Mochida, A., Yoshie, R., Kataoka, H., Nozu, T., Yoshikawa, M., Shirasawa, T. 2008. AIJ guidelines for practical applications of CFD to pedestrian wind environment around buildings. Journal of Wind Engineering and Industrial Aerodynamics 96(10-11), 1749-1761.

Wilson D.J., 1989. Airflow around buildings, ASHRAE Handbook of Fundamentals, pp. 14.1-14.18.